ChemComm

Accepted Manuscript

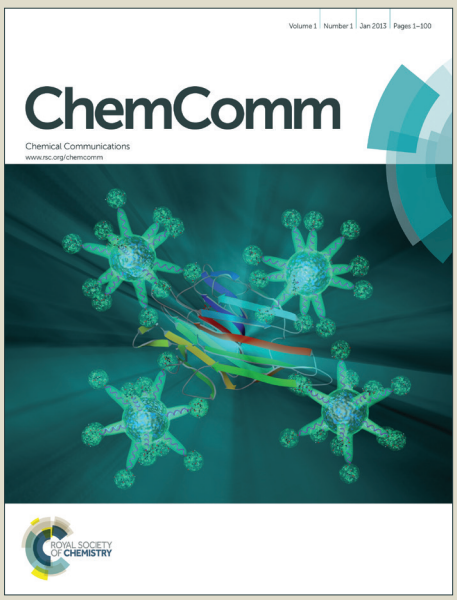

ROYAL SOCIETY OF CHEMISTRY

www.rsc.org/chemcomm

Chemical Communications RSCPublishing

FEATURE ARTICLE

Building With Bubbles: The Formation of High Surface Area Honeycomb-like Films via Hydrogen Bubble Templated Electrodeposition

Cite this: DOI: 10.1039/x0xx00000x

Received ooth August 2014,
Accepted ooth

DOI: 10.1039/x0xx00000x

www.rsc.org/

Blake J. Plowman, Lathe A. Jones* and Suresh K. Bhargava*

Centre for Advanced Materials and Industrial Chemistry (CAMIC), School of Applied Sciences, RMIT University, GPO Box 2476V, Melbourne, VIC, 3001, Australia.
** Email: lathe.jones@rmit.edu.au, suresh.bhargava@rmit.edu.au.*

While the evolution of hydrogen gas is often a troublesome process accompanying electrodeposition, this feature can be exploited to template the growth of highly porous surfaces. This process, known as the dynamic hydrogen bubble template (DHBT) method, can be utilised to create a wide range of macroporous films with nanostructured pore walls. This feature article presents an overview of the status of the DHBT technique, highlighting preparation techniques and emerging applications.

1. Introduction

The preparation of materials with both a high specific surface area and controlled morphology is of vital importance in a diverse range of applications, particularly catalysis,[1] sensing,[2] energy,[3] and for the control of surface dependent properties such as hydrophobicity.[4] Porosity ensures economical use of materials, especially important when noble metals are used, and fine structure on the nanoscale is intimately related to activity in surface confined processes such as catalysis.[5] Much work has been dedicated to understanding the parameters that control the morphology and surface area of inorganic materials[6] and metals[7] by electrodeposition. Electrodeposition can be used to control the shape of nanomaterials, such as supported nanoparticles,[8] and influence the growth and nucleation mechanisms that dictate the grain sizes and morphology of bulk materials or films.[9] Electrodeposition is most convenient from aqueous solution, and the instinct of an experimentalist is to work within the solvent window of the electrolyte, where reduction of the solvated metal ions takes place without interference from solvent decomposition. In aqueous solution at sufficient cathodic overpotential, H^+ is reduced to H_2, which bubbles off the growing metal deposit, disrupting the growth mechanism (reactions **I (Ia-c)** and **II** and Fig. 1). These H_2 bubbles can actually be used as a dynamic template during the electrodeposition process. Macropores in the micron size range are caused by growth of the metal around the bubbles generated on the surface, maximising the specific surface area. The stirring action of the bubbles affects the hydrodynamic conditions near the surface of the electrode, profoundly affecting the subsequent nanostructure of the material. Growth structures such as dendrites and foams, and the generation of active surface sites, are a consequence of both the H_2 evolution and the high overpotential employed. The advantage of the Dynamic Hydrogen Bubble Template (DHBT) technique is that it is clean and efficient, allowing access to porous morphologies without the use of an additional organic or inorganic templates. The first detailed studies were undertaken on Cu and Ni, and accelerated interest in the last few years has led to a larger range of metals, including extension to bimetallic films, and various post-deposition treatments to enhance performance in key applications. The versatility and simplicity of the method, coupled with the enduring need for reliable access to porous films, leads us to believe this technique will continue to grow in the near future. In this article we will review the current state of the art with selected examples of recent advances in the literature, and present a case for further development of the DHBT technique for extension to new applications.

$$2H^+_{(aq)} + 2e^- \prod H_2 \qquad \textbf{I}$$

$$H^+_{(aq)} + e^- \prod H_{(ads)} \qquad \textbf{Ia}$$

$$H^+_{(aq)} + H_{(ads)} + e^- \prod H_2 \qquad \textbf{Ib}$$

$$2H_{(ads)} \prod H_2 \qquad \textbf{Ic}$$

$$M^{n+}_{(aq)} + ne^- \prod M_{(s)} \qquad \textbf{II}$$

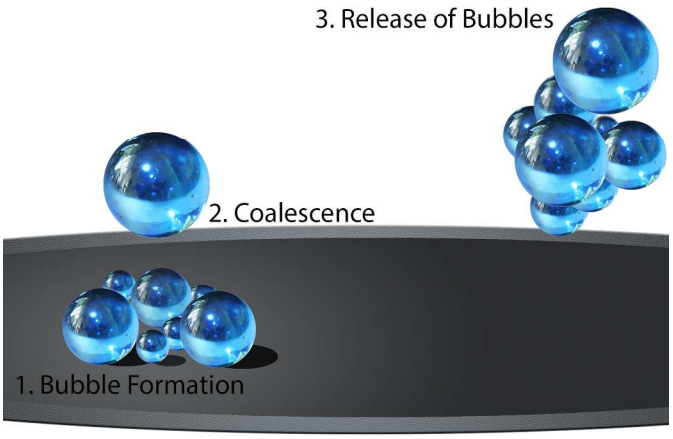

Fig. 1 Schematic showing the formation, coalescence and release of hydrogen bubbles from the electrode surface during the DHBT preparation of honeycomb-like films. H_2 evolution (equations Ia-c) occurs in parallel to M deposition (equation II).

2. Synthesis methods and conditions.

2.1 Mechanism and Experimental Considerations.

A basic understanding of the mechanism of bubble generation off the surface of an electrode, and the effect this has on the growth of the metal is required to appreciate the DHBT technique. The rate of H_2 evolution varies with the substrate metal, with trends in exchange current densities having been extensively studied,[10] leading to the traditional "Volcano curve" based upon the experimental exchange current densities plotted as a function of hydrogen chemisorption energy. Exchange current densities for the metals commonly electrodeposited, from fast to slow kinetics are (log i_0/ Acm^{-2}) Pt (-3.1)> Pd (-3.0)> Ni (-5.21)> Cu (-5.37)> Au (-5.4)> Ag (-7.85).[10] Metals such as Pt and Pd will thus generate higher volumes of H_2 at a specific overpotential. At H_2 nucleation sites on the electrode, which have been experimentally observed to occur at active sites such as surface irregularities,[11] defects and edges,[12] H_2 is generated through the equations indicated by (Ia), (Ib) and (Ic), though the precise mechanism can vary depending on the electrode material and conditions.[13]

In addition to aqueous acids such as H_2SO_4 or HNO_3, aqueous NH_4Cl solutions may also be used to generate H_2 off an electrode surface (equation III), though with the inconvenience that a range of side reactions can occur,[14] (for example production of NH_2Cl, $NHCl_2$ and complications from Cl_2 evolution at the anode is some cell configurations). Dissolved NH_3 is capable of altering the chemistry of the dissolved metal species in the diffusion layer. [14]

$$2\ NH_4^+ + 2e^- \prod H_2 + 2NH_3 \qquad \textbf{III}$$

Vogt[15] and Diez and Tawfik[16] have studied the theoretical and practical factors that govern H_2 evolution at polarised electrodes. Generation of gas bubbles off the surface of the electrode involves three steps: nucleation, growth and detachment. Electrochemical generation of H_2 gas by equation **I** can either lead to the H_2 diffusing to the bulk solution, or flux to the liquid-gas interface of a bubble leading to bubble growth. High overpotentials, as is customary with the DHBT technique, will readily lead to super-saturation of the solution near the electrode with H_2, resulting in heterogeneous nucleation.[17] The bubble will grow while still in contact with the electrode during its residence time on the surface, with a decreasing contact angle during growth until detachment. Small bubbles in the electrolyte are attracted to the larger bubble and can coalesce. The residence time of the bubble, and hence its size, is affected by its ability to coalesce, and by surface energy of the growing surface, which is dependent upon the morphology, material, and overpotential, and is still not yet completely understood.[18] There is thus a complex relationship between the interaction of the interfacial tensions between the 3-phase system – electrode/electrolyte/gas, and adjustment of experimental parameters is undertaken in line with some general rules for bubble behaviour outlined below.[15e]

Bubbles are insulating and so their presence will reduce effective surface area through[19] a surface blocking effect,[20] affecting the area available for the concomitant metal reduction represented by equation II. As such, the actual current density (j), which exerts control on the growth morphology of the metal, will be higher than the nominal current density (I/A), which is the applied or measured current (I), divided by the surface area (A).[15e] If θ is the inactive fraction of the electrode surface:

$$j = (I/A) / (1-\theta)$$

θ depends upon the number of simultaneously adhering bubbles, their rate of growth, and their size as they leave the electrode.[21] Bubble density increases with current density, as the residence time of the bubbles decreases due to instability of larger bubbles at higher growth rates. With this increase in bubble coverage, local current density increases. Each nucleation site tends to hold a small pocket of entrapped gas, which remains after bubble detachment, and promotes bubbles being evolved off the same site.

Surfactants and additives will critically affect bubble behaviour, with surfactants residing at the bubble-liquid interface impeding coalescence due to reduced surface tension. Even small surfactant concentrations will have an effect, with large surfactant concentrations preventing coalescence almost completely. The smallest amount of ethylene glycol will also reduce bubble size, as will sodium sulphate, which also tends to

disrupt average bubble diameter.[22] Changes in sulphuric acid concentration, often used as a H^+ source by the DHBT method, has been reported to have minimal effect directly on bubble release diameter.

Metal electrodeposition can occur around the bubble, as was originally directly observed by Tsai and co-workers.[23] The diffusion layer width, which affects the growth mechanism and subsequent morphology of the electrodeposited metal, will decrease due to the hydrodynamic effect of the evolving H_2.[21] In fact vigorous H_2 evolution has a similar effect on mass transfer as intensive mechanical stirring. The pores in the electrodeposited film will be approximately the same size as the release diameter of the bubbles, with the pore density of the film predominately determined by bubble behaviour.

An elegant summary of the variation of pore size with distance perpendicular to the electrode surface was presented by Ye and co-workers[24] (Fig. 2). Here it can be seen that for short distances from the electrode surface, relatively small pores are formed, which increase in size as the film grows. This is seen indirectly from microscopic images of the surface (Fig. 2b), where significantly smaller pores are observed underneath the overlying larger pores. The larger pore size as the film grows off the surface can be explained by the increased coalescence of bubbles, as smaller bubbles coalesce in the confined space of the initially formed pores, indicating that in 3D structures bubble size increases during the deposition in response to the changing morphology. This "Stack up layer" model leads to films of initially small pore diameter followed by larger diameter as perpendicular growth proceeds. In the study by Ye, top layers were approximately 2-3 times larger in pore size than lower layers (20-35μm at the bottom compared to 60-90 μm near the surface of a 3D film).

The size of the pores in the micron size range will thus be determined by the bubble behaviour, but the fine morphology of the metal film will be determined by the nucleation and growth mechanism of the metal, which is dependent upon the hydrodynamic conditions and overpotential. Nikolic and co-workers studied the effect of electrodeposition conditions on the morphology of Cu deposits.[25] Dendritic deposits are most likely to be formed in a diffusion limited regime, and they observed that in the presence of H_2 evolution the morphology of the deposit is greatly affected by the decrease in the diffusion layer thickness. They observed that an increase in the overpotential required for diffusion limited growth is observed compared to a quiescent solution. This led to the term "effective overpotential" being phrased,[26] where there is a change in hydrodynamic condition near the electrode, and of subsequent electrodeposited morphologies, due to the decrease in the thickness of the diffusion layer and an increase in the limiting diffusion current density. Cherevko and Chung made observations based upon their deposition of porous Pd that the decrease in the diffusion layer thickness causes an increase in the diffusion limited current, with a subsequent decrease in the initiation overpotential.[27] This phenomenon allows access to high surface area films of metals that typically display slow kinetics for electrodeposition.

From a practical point of view, due to an increase in H_2 evolution rate with overpotential, pore density increases with current density. This higher current density will lead to smaller pores, and then eventually to foam type materials that are not structurally sound as wall thickness decreases.

The working electrode material, shape, size, and orientation may all affect the bubble behaviour, and as such an experimental setup must be devised that allows these factors to be constant while adjusting parameters to achieve a film with a favourable morphology. A traditional 3-electrode setup is preferable for precise control of overpotential. The final structure of the film will thus rely on this interplay between bubble behaviour, and the effect the bubbles have on the nucleation and growth of the metallic film.

There is no standard experimental setup to allow repeatable generation of films, though some controlled studies have allowed a better understanding of bubble release and growth mechanisms[28] using externally imposed hydrodynamic conditions, although this procedure has not been adopted as common practice. The key parameters that can be identified are: H^+ source and concentration (acid or NH_4Cl), overpotential (or current density), substrate material and metal salt concentration/solution chemistry. Variation of one of these at a time enables the experimentalist to find the conditions that lead to a porous structure, as long as other factors that may affect bubble behaviour (T, surface tension etc.) are kept constant or closely controlled. It is also desirable to have a cell setup where the electrode positions, in particular the working electrode, are kept constant, with systematic variation of the key parameters identified above taking place under identical conditions. The morphology obtained under a set of conditions can thus be related to our understanding of bubble behaviour and electrochemical growth mechanisms, with examples of this becoming apparent in the following sections. Bubble behaviour on the working electrode will vary with orientation, as a downward facing surface may trap bubbles, and in our experience vertical samples may lead to inconsistencies if the upper surface of the substrate is close enough to the electrolyte-outside gas interface to affect bubble behaviour. Substrates either facing up or vertical (deep in solution) tend to give the most repeatable results. Initial dimensions are usually surface areas of less than 1 cm^2, though scale up has been promising in some instances.[22] Care must always be taken that substrate preparation is consistent to ensure the active sites most likely to nucleate H_2 are repeatable on successive experiments. Initial deposition conditions are often an excess of acid (0.1 to 0.5 M), with variation of the metal concentration in the mM range (1 to 100). Copper concentrations are often considerably higher (up to 0.4 M for honeycomb Cu), but such high concentrations of noble metals are not always practical. With these background theoretical and practical considerations in mind, the following sections will outline the main factors that affect the properties of the porous films formed, and their applications.

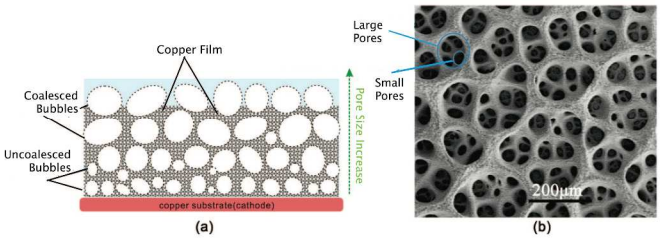

Fig. 2 "Stack up model" (a) Schematic and (b) SEM image of copper demonstrating the effect of hydrogen bubble coalescence on the pore structure of honeycomb-like films. Reproduced by Permission of the Electrochemical Society. [24]

2.2 Monometallic Surfaces Created Using the DHBT Method

While the electrodeposition of metal surfaces with accompanying hydrogen evolution has been known for a long time, for example work in the 1970s was undertaken on the formation of copper powders,[29] little was known on the structure of the deposits or how they might be tailored.

A clearer picture of such work was presented later by Marozzi and Chialvo,[30] dating to 2000-2001. Their work involved the electrodeposition of porous nickel films for electrocatalysis, particularly for use with the hydrogen evolution reaction (HER). It was noted that hydrogen adsorption commonly accompanies nickel electrodeposition, and for this reason the surfaces were heated under mild conditions (70 °C for 12 hours) to remove the occluded hydrogen. The porous nickel surfaces formed in this manner were found to possess improved electrocatalytic activity when compared with Raney-Nickel deposits.

A range of groups then looked to extend to other metals. Amongst the most investigated has been honeycomb-like copper surfaces, with much of this work performed by Popovic, Nikolic and co-workers. Copper presents an appealing material for deposition using the DHBT method, as it provides an inexpensive route to the synthesis of high surface area films which may be either used as prepared, or further modified to suit a specific application. Also, Cu has been used as a model in nucleation and dendritic growth studies, leading to a good understanding of its deposition behaviour.[31] An example of such a honeycomb-like Cu surface is shown in Fig. 3, as reported by Liu and co-workers.[32] The porous nature of the electrodeposited film can be readily observed from the SEM images in Fig. 3a-b, where pores of approximately 30 μm are visible within an interconnected network of pore walls. While the pore sizes can be seen to have a degree of variability, as a result of variations in the sizes and residence time of the H_2 bubbles, the variation in this instance is modest. Also of note is the relative homogeneity of the surfaces across large areas (note the 100 μm scale bar in Fig. 3a), demonstrating the potential to upscale the geometric electrode area for use in applications. The morphology of the pore wall network is evident from the side-on images in Fig. 3c-d, where the electrodeposited Cu extends some 50 μm from the underlying substrate in dendritic-like, nanostructured growths. Such structures provide greatly enhanced surface areas compared to the underlying substrate (often hundreds of times higher), providing a multitude of surface sites to interact with reactant species across a range of applications.

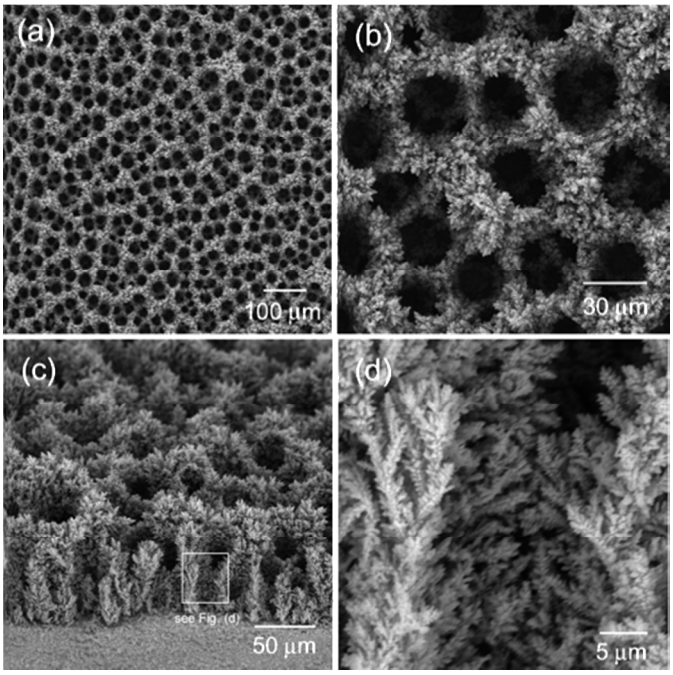

Fig. 3 SEM images showing top-down (a,b) and cross-sectional (c,d) views of a honeycomb-like Cu surface (Reprinted with permission[32]). Copyright 2004, American Chemical Society).

Much of the work on controlling and understanding the formation of these structures has been performed for the honeycomb-like Cu system, and for detailed overviews the reader is encouraged to consult reviews by Nikolic and co-workers.[33]

A number of different electrodeposition techniques have been utilised, with constant potential[12, 25-26, 28a, 34] (potentiostatic) or constant current[24, 32, 35] (galvanostatic) methods the most common methods of electrodeposition, which broadly speaking produce similar morphologies. Later work by Nikolic and co-workers has been directed towards pulsed deposition methods, [34a, 34b, 35a, 35e, 36] where the applied reductive potential (or current) is interspersed with brief rest periods. This method was developed to control the size and residence time of the H_2 bubbles, in turn influencing the size of the pores in the final structure. Pulsed methods were also extended to reversed current methods,[35a, 36b] where the rest pulse is instead stepped to a potential which drives the partial dissolution of the electrodeposited Cu.

The choice of electrode surface for the electrodeposition is an important factor which influences the morphology of the resulting film. A comparison of several such electrodes was presented by Najdovski and O'Mullane,[37] who demonstrated

the importance of the underlying electrode on the basis of the on-going evolution of hydrogen on exposed regions of the surface. For instance, it was observed that smaller pores for porous copper were produced on Au substrates compared with Cu (owing to the higher HER activity on the evaporated Au film compared to the Cu foil used), while depositions on glassy carbon and Pd did not form the same well-ordered structures. Catalytic activity for the HER and ferrocyanide reduction varied for porous copper deposited onto different substrates, indicating the importance on the morphology and activity that the initial substrate can impose on the film. Other reports of surfaces utilised for electrodeposition, an indication of the versatility of possible end uses for the DHBT method, include evaporated films,[38] foils,[39] microelectrodes,[34h] wires,[34f] disc[40] or screen printed electrodes,[41] with honeycomb-like architectures successfully obtained for all these substrates. The roughness of the underlying electrode surface has also been investigated by Kwon and co-workers,[35e] who observed that electrodes first roughened by electrodeposition (under much less vigorous conditions than employed in the DHBT method) significantly altered the morphology of Cu electrodeposited using the DHBT technique.

Further control of morphology can also be achieved by the inclusion of shape directing agents in the electrodeposition bath. This was demonstrated by Kwon and co-workers,[35d] who investigated the effect of ammonium sulphate and benzotriazole (BTA) on the electrodeposition of copper. As shown in Fig. 4a, a porous copper surface was formed in the absence of any shape directing additives, whose nanostructure (inset) was characterised by the presence of dendrites and flower-like growths, in keeping with prior work on copper electrodeposition. The addition of ammonium sulphate (Fig. 4b) had a marked effect on the morphology of the deposits, with a thickening of the pore walls visible from the low magnification image. The inset shows that these pore walls are composed of much finer nanorod-like structures. This material displays a similar macroporous structure to that formed in the absence of additives (Fig. 4a), however it should exhibit different activity in applications such as (electro)catalysis. A much different morphology was attained when BTA was used, with the low magnification image (Fig. 4c) showing a much lower degree of pore formation. Likewise the influence on the nanostructure is pronounced and this was attributed to the interaction of Cu(I) species with BTA adsorbed on the growing copper electrodeposit. Interestingly a synergistic effect was found in the case of electrodepositing in the presence of both ammonium sulphate and BTA (Fig. 4 d). Here the honeycomb-like structure is again formed, although the dimensions of both the pores and the pore walls are noticeably decreased, leading to a surface with a higher density of pores. This study demonstrates the ability to tune the morphology of the films both on the micro- and the nanoscales. Interestingly, while similar studies have shown the influence of shape directing agents on copper electrodeposition under far less vigorous conditions, it is noteworthy that such control over the morphology of the deposits can be achieved given the particularly rapid nature of the electrodeposition, showing the speed at which the shape directing agents can act. A range of other shape directing agents have also been reported to successfully adjust the nanostructured and/or macroporous morphology of electrodepositions employing the DHBT method. Halides are common examples of this (including NaCl,[24] HCl,[32, 35j, 35k, 35m] NaBr, [35c] KI[42] and NH_4Cl[34k]), whilst in other cases additives such as mercaptopropyl siloxane,[28a, 35e, 35k] polyethylene glycol (PEG)[35c, 35e, 35k] and cetratrimethylammonium bromide (CTAB)[35h, 35l] have also been employed. Such examples illustrate the rich variety of approaches which can be used to tailor design the surfaces.

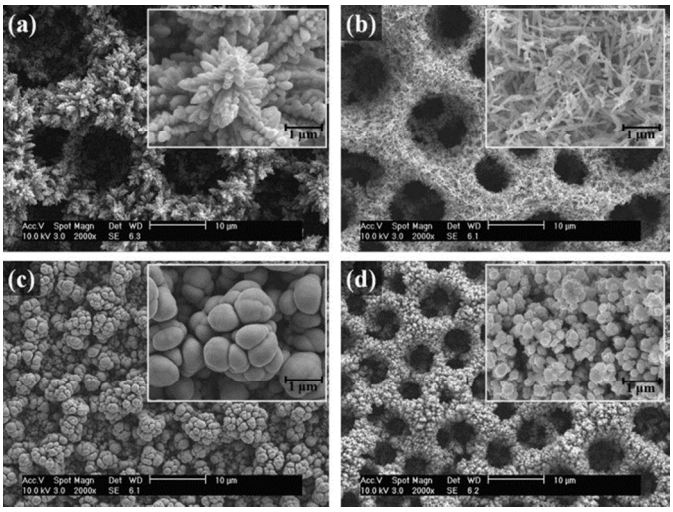

Fig. 4 SEM images showing the electrodeposition of honeycomb-like copper surface (a) and with the addition of ammonium sulphate (b), benzotriazole (c) or ammonium sulphate and benzotriazole (d) (Reprinted with permission[35d]. Copyright 2011, Elsevier Ltd.).

In addition to the relatively large number of papers published on honeycomb-like Cu to date (>35 papers), other monometallic porous surfaces synthesised using the DHBT method have been appearing at a steady rate. This includes the initial work in this area on porous Ni by Marozzi and Chialvo.[30] An interesting variation was reported by Xia and co-workers, who formed porous silica networks using similar conditions to those for monometallic surfaces. These depositions relied on a different mechanism compared to the metallic surfaces, with the silica forming through a precipitation reaction caused by the intense evolution of hydrogen raising the local pH near the electrode surface. These depositions were performed in the presence of enzymes including glucose oxidase (GOX)[35l] or horse radish peroxidase (HRP),[43] in order to encapsulate the enzyme in the porous structure as an immobilized bioactive material.

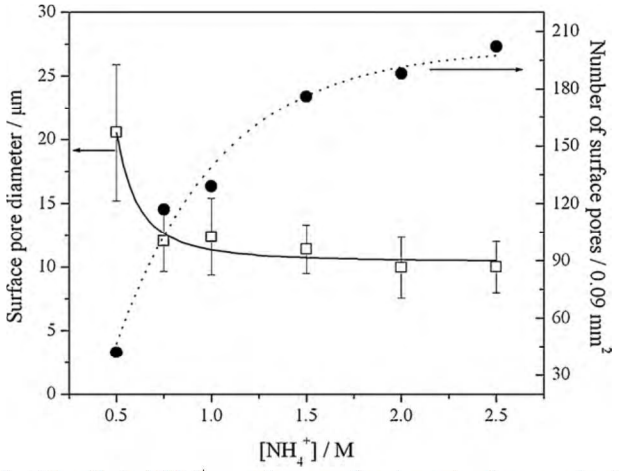

Fig. 5 The effect of $[NH_4]^+$ on surface pore diameter and surface pore density for a Ag film [44], showing decrease in pore diameter and increase in pore density within increasing $[NH_4^+]$ (Reprinted with Permission, Elsevier B.V. 2010.)

While many of the early studies on porous metallic surfaces formed using the DHBT method were largely limited to Cu or Ni, much of this work was shaped by a desire to understand the fundamental nature of how the morphologies of the structures could be fine tuned, rather than investigating how broadly applicable this procedure is for the deposition of a wide range of metals. A turning point in this field occurred with work by Cherevko and co-workers, who demonstrated that honeycomb-like Ag structures could be readily formed.[44-45] Instead of using acid as a proton source for the H_2 bubble formation as is customary in earlier work, they instead adopted NH_4Cl, which also had the advantage of stabilising the deposition solution, and was required in at least 0.25 M concentration to form honeycomb-like structures. This work showed that noble metals could be synthesised with similar macroporous architectures and nanoscale features as Cu and Ni, leading to desirable materials for catalysis. Fig 5 shows experimentally how the variation in the $[NH_4]^+$, which in this case acts as a proton source for hydrogen evolution, affects the pore diameter and the surface pore density. The pore size reduces at higher $[NH_4^+]$, indicating a reduced bubble break off diameter. As $[NH_4^+]$ is increased, the pore wall thickness (or interpore distance) is reduced, which eventually leads to foams which are unstable.

While the electrodeposition of a honeycomb-like silver surface had been demonstrated, the electrochemical formation of honeycomb-like gold using the DHBT method was discounted in the literature, due to the lower overpotential for H_2 evolution and higher equilibrium potential.[46] Porous gold was instead fabricated using a galvanic replacement approach (as will be discussed in the following section), with porous copper acting as a scaffold for the galvanic replacement of gold.[46] Direct electrodeposition of gold would be beneficial, as it would reduce the preparation time as well as the possible influence of any remaining template. Such a synthesis was reported for the first time by our group, with the electrodeposition forming porous gold honeycombs with active sites on gold substrates.[47] As was discussed earlier for the case of copper, the deposition of gold was sensitive to the presence of anions in the deposition solution, which in this instance was through electrodeposition from a gold chloride or a gold bromide salt. In the former case dendritic growths were observed with short branches, while in the latter dendrites were still seen but a much higher proportion of long (~20 µm) rods, with short protruding branches were formed. The choice of underlying electrode surface may suggest why a honeycomb surface was not produced in earlier attempts, as the underlying glassy carbon surface presents a less active surface for hydrogen evolution than evaporated gold,[48] and depending on its pre-treatment and history it may also have a higher degree of heterogeneity. The fabrication of porous gold was then also described by Cherevko and co-workers[49] who employed different conditions including the use of NH_4Cl as a proton source, as well as further reports by other groups.[42, 50]

The electrodeposition of Bi has been studied by Yang.[28b] These depositions were of note not only for the use of the DHBT method for the deposition of metal dendrites with a large deposition overpotential, but because they also provided a facile manner to study the effect of hydrogen bubbles staying adsorbed to the surface over extended periods of time (referred to as 'stagnant' bubbles). This was achieved due to the positioning of the electrode, facing down into the solution and therefore trapping the *in situ* generated bubbles against the electrode surface. Another interesting factor of these depositions was that the growth of the hydrogen bubbles was favoured on the glassy carbon support as opposed to the growing Bi electrodeposit, which was possibly due to the evolution of hydrogen occurring at less negative potentials for glassy carbon compared with the growing Bi dendrite.

Following the electrodeposition of Bi, the electrodeposition of noble metallic surfaces was again addressed by Cherevko and co-workers through deposition of porous Pd.[27, 51] These Pd structures are shown in figure 6, with a large number of small pores evenly distributed, and small particle-like growths evident on the nanoscale. As with other reports of monometallic surfaces, the size of the pores can be readily tuned by varying the deposition time (Fig. 5a-c for 1 min, 2 min and 4 min, respectively), increasing the average pore size in accordance with the "stack up model". The synthesis of porous Pd has since been revisited by a number of groups, with a view to investigating the electrocatalytic activity of these promising surfaces towards fuel cell-related reactions.[52]

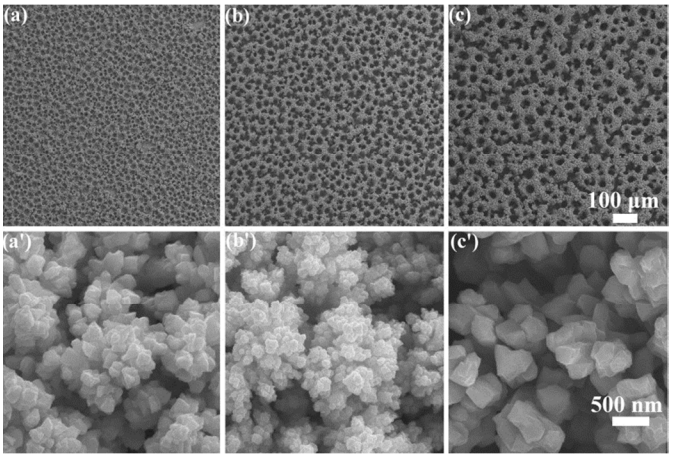

Fig. 6 Honeycomb-like Pd surfaces electrodeposited for 1 min (a), 2 mins (b) or 4 mins (c), along with their corresponding higher magnification images (a'-c') (Reprinted with permission[51]. Copyright 2010, Elsevier B.V.).

Cherevko and co-workers then investigated the electrodeposition of Pb, given its high chemical activity and its use in superconductors and batteries.[53] Through variation of electrodeposition parameters they determined conditions which can produce similar morphologies to those discussed above for other metals. Additional tuning of the nanostructures was performed by the inclusion of sodium citrate, to influence the crystal growth. In this manner wire-like morphologies were attained, whereas in its absence particles and particle-covered rods formed. While this work was the first report of the electrodeposition of porous Pb using the DHBT method, a similar method was reported by Huang and co-workers.[54] This method involved the formation of porous Pb and Sn by the application of a strongly cathodic potential of bare metal electrodes in NaOH. This resulted in the formation of metal hydrides, which then decomposed back to their metallic forms. This process was also templated by hydrogen bubbles generated *in situ*, forming a porous film similar to that electrodeposited by Cherevko and co-workers.

The wish to generate porous surfaces of the most catalytically active metals led to the preparation of honeycomb-like Pt, reported by our group.[28b] The motivation for this work was to study whether the synthesis of platinum films differed from that of other metals given its high activity towards hydrogen evolution. It was noted that the composition of the deposition bath displayed a marked effect on the morphology of the surfaces, and the deposition of honeycomb-like Pt was successfully demonstrated at relatively high Pt(II) concentrations (50 mM), although lower concentrations of Pt(IV) salts were successfully used later by Li.[55]

Another material which has been electrodeposited using the DHBT method is Sn. This was first reported by Hong and co-workers who fabricated porous SnO_2 foams composed of networked dendrites.[56] An annealing procedure was undertaken after the Sn electrodeposition at 700 ºC for 1 hour in air to form SnO_2. Under the conditions employed in this work sizeable differences in the macroporous structure are visible in increasing the electrodeposition time from 5s to 10s, especially visible through a large increase in the pore wall thickness. The nanostructures formed are highly branched rods, with the secondary branches also displaying rod-like growths. Similar morphologies were also reported by Cao and co-workers, who formed porous Sn/SnO_2 surfaces.[57]

The electrodeposition of Ru has recently been reported by our group.[58] This involved electrodeposition using conditions that favoured the growth of metallic ruthenium dendrites. This is the first report of dendritic growth of ruthenium by electrodeposition, whose morphology is difficult to control due to the slow kinetics of Ru^{3+} reduction. The high overpotential and hydrodynamic conditions of the H_2 bubbles were able to force the growth of dendrites, although three-dimensional honeycomb structures were not observed. This work, combined with observation of low melting point metals such as Pb[49a] may also show broader application for the electrodeposition of metals with slow kinetics, especially where dendritic growth is desirable but is difficult to achieve through other routes.

A final example of a monometallic material formed by the DHBT method is Co. While the templating effect of hydrogen bubbles on Co deposition was noted by Jović and co-workers,[59] later work by González-Buch and co-workers demonstrated the electrodeposition of more ordered Co (as well as Ni and CoNi) porous surfaces.[60] For the case of Co a large number of clustered growths were observed across the honeycomb-like surface, which displayed clear evidence of the templating effect of the H_2 bubbles.

2.3 Synthesis of Bimetallic Surfaces Based on the DHBT Method

A significant advantage of the DHBT methodology is the ease of fabrication for bimetallic surfaces. This opens up scope for improvements in applications such as catalysis, where synergistic effects can be leveraged to tune activity. Preparation of bimetallic surfaces can be classified by whether the secondary metal is added through electrodeposition on top of an existing porous template, by co-electrodeposition, or by electroless reduction processes such as galvanic replacement or spontaneous decoration.

2.3.1 Electrodeposited on top

Bimetallic surfaces can be formed by electrodeposition on top of a template previously formed by the DHBT method. This is a simple fabrication procedure, as the desired pore structure and morphology may be achieved using a well-studied system such as Cu. This has been achieved for the case of Ni, Sn and Si on honeycomb-like Cu, with a variety of reasons given for choosing the two-step electrodeposition procedure, rather than utilising a direct electrodeposition approach. Mechanical adhesion of the structures to the electrode surface is a common motivation. For example Perez-Herranz and co-workers[61] prepared Ni electrodes by deposition on top of a Cu honeycomb template for water electrolysis. In the case of Si deposition, the honeycomb-like Cu instead provided sufficient mechanical

strength to attach the Si overlayer, as well as providing a high surface area framework, acting as a current collector and reducing the structural stress associated with its use in Li-ion batteries.[35g] Similarly, for Sn electrodeposition a Cu deposition protocol was selected so that a porous surface composed of grape-like nanostructures was obtained, as it was thought that the mechanical adhesion of dendritic growths would not be sufficient for Li-ion battery applications.[35e, 62] It should be noted that for the cases listed relatively large amounts of material were electrodeposited on the supports, and while some modifications on the overall porous morphology are visible the nanostructured morphologies are often altered post-electrodeposition.

The use of honeycomb-like films as support structures for further modification by electrodeposition is also compatible with other deposition procedures, such as co-electrodeposition (as will be discussed in the next section). This is highlighted by work by Sun's group, who electrodeposited SnCo on porous Cu frameworks.[39] In this case the mechanical adherence of the Cu support was determined to be insufficient for the use of the structures in Li-ion batteries, so the co-electrodeposition was performed on annealed honeycomb-like surfaces. While this latter treatment lead to large changes in the nanostructured morphology, the overall porous structure was maintained and provided a suitable support.

Conformal deposition of thin layers on top of films generated by the DHBT method has not been studied and remains an area that is open. It is assumed that thin layers could be deposited by either posterior non-diffusion limited electrodeposition procedures, or by physical techniques to create films with a surface that retains the structural integrity and high surface area of the underlying honeycomb material.

2.3.2 Co-electrodeposition

Co-electrodeposition involves the dissolution of two metallic salts in the deposition bath, resulting in the direct formation of a bimetallic honeycomb-like material. This was illustrated by work performed by O'Mullane and co-workers, who investigated the electrodeposition of CuAu,[63] CuPd[64] and CuAg.[65] In the case of CuAu, variations are evident in the macroporous structure of the surfaces (Fig. 7) as the deposition proceeds in the absence of $KAuBr_4$ (Fig. 7a) and then with increasing concentrations of $KAuBr_4$ (Fig. 7b-d). These latter samples show greatly reduced pore sizes as compared with the Cu-only surface, which may be attributed partly to the enhanced evolution of hydrogen on the structured, active Au compared with Cu. It has been shown that Au forms structures that are very active for hydrogen evolution when deposited as dendritic, active structures by the DHBT technique,[47a] giving rise to a higher H_2 evolution rate than suggested by the trend in exchange current density on flat polycrystalline electrodes. The structure of the growing surface will thus affect the H_2 evolution and subsequently the structure in ways that are difficult to predict before a range of films are prepared and examined experimentally. The nanostructure of the deposits was also found to vary with increasing concentrations of $KAuBr_4$ in the deposition solution, and the amount of Au in the film increased from 0% in Fig 7a to 0.5 % (7b), 0.7 % (7c) and 1.2 % (7d), showing that even small amounts of noble metal incorporated into the film can greatly affect the morphology. The structure shifted from dendritic growths in the absence of $KAuBr_4$ (in agreement with prior studies on monometallic copper honeycomb-like) to cube-like structures and finally block-like crystallites and thin plate-like deposits at higher concentrations of $KAuBr_4$. Notably these latter morphologies are different to those reported previously for the electrodeposition of monometallic honeycomb-like gold, where dendritic and rod-like growths were favoured. Also of note is the surface chemistry of the CuAu films, where it was found that a Au (I) oxide species remained within a Cu_2O framework. This unusual species was found to be particularly beneficial for catalytic and electrocatalytic applications, and remained active over extended testing periods.

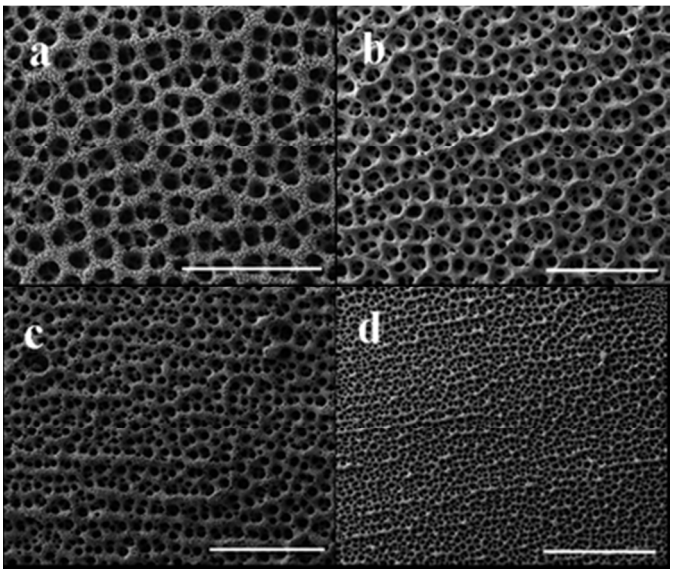

Fig. 7 CuAu honeycomb-like structures electrodeposited under similar conditions but in the presence of 0 (a), 5 mM (b), 10 mM (c) or 20 mM (d) KAuBr4. (Reprinted with permission[63]. Copyright 2012, The Royal Society of Chemistry).

Co-electrodeposition has also been used in the synthesis of honeycomb-like Ru films.[66] Owing to the difficulty in preparing porous Ru using a direct DHBT approach,[58] Chung and co-workers prepared a RuCu alloy first. This created a highly porous (23.5 m^2g^{-1}) structure (Fig. 8a) extending tens of micrometers from the surface (Fig. 8b), whose pore walls were composed of dendritic structures (Fig. 8c) and blossom-like (Fig. 8d) nanostructures. Since the presence of Cu in the final film was not desired, this was removed from the material using an electrochemical de-alloying approach. This led to a porous Ru based material composed of hollow nanostructures (Fig. 8e-f), with a high surface area (207.5 m^2g^{-1}).

Other bimetallics that have been prepared by the DHBT technique include CuSn[67] and a range of bimetallics containing

Ni (NiSn,[68] NiCo,[69] NiCu[70]), Pd (AgPd,[71] PdNi[52b]) and Pt (PtPd,[41] AuPt,[72] CuPt[73]).

A further interesting example of co-deposition is NiCoFe.[74] This work, by Rafailović and co-workers, synthesised Ni-rich denritic alloys consisting of $Ni_{50}Co_{30}Fe_{20}$. This alloy formed as highly dendritic growths, although under the conditions presented the overall morphology resembled the growth of large dendrites with a high degree of size distributions, with the overall templating effect of the hydrogen bubbles less evident than in other cases. Similar results were also found by Sun and co-workers,[75] who electrodeposited FeSnSbP composites using a co-reduction method. A high surface coverage of fern-shaped structures resulted, and although again the imprint of the hydrogen bubbles was not evident the material was tested for application in Li ion batteries. While both of these studies do not show the same H_2 bubble templating as evident in most mono- or bimetallic surfaces, they clearly demonstrate that multimetallic surfaces can be formed readily with interesting morphologies. The DHBT method also provides a straightforward route to control the composition of the electrodeposits, as the high reduction potential may simplify the reduction of all metal species to diffusion-controlled cases and avoid any kinetic barriers hindering the growth of particular elements. Once this diffusion-controlled case is established the composition of the electrodeposit can be readily tailored by altering the concentration of the deposition bath, providing a ready route to fabricate multimetallic surfaces.

2.3.3 Galvanic Replacement

A versatile method to convert a monometallic material into a bimetallic is galvanic replacement. This involves the replacement of a template material with an appropriate metallic salt, driven by the potential difference of the related redox species. Galvanic replacement has lead to the fabrication of a large number of interesting nanostructured materials,[76] with the added benefit of being able to decorate or replace a relatively inexpensive, non-noble metal template with a more active, but expensive noble metal such as Pt, Pd or Au. This method has also been applied to scaffolds formed through the DHBT method, with the reduction of gold driven by the oxidation of the copper template, as reported by Xia and co-workers in 2007.[46]. The copper surface has the advantage of providing both the overall porous structure, although it should be noted that galvanic replacement can introduce changes in the nanoscale morphology. This may be desirable for particular applications, providing a valuable synthetic tool. During the galvanic replacement process, oxidation (dissolution) of the substrate occurs as one half reaction, with reduction (deposition) of ions of a different metal in solution being the other half reaction, driven by the electrochemical potential difference in the two half reactions. As the substrate is a sacrificial template, and plating of a metal from solution takes place, the structure may closely resemble the template on the macroscale, but the nanoscale morphology will be affected, with often a slight increase in dimensions due to the additive effect of electroless plating. The control of morphology by galvanic replacement has recently been reviewed by Xia and co-workers.[77]

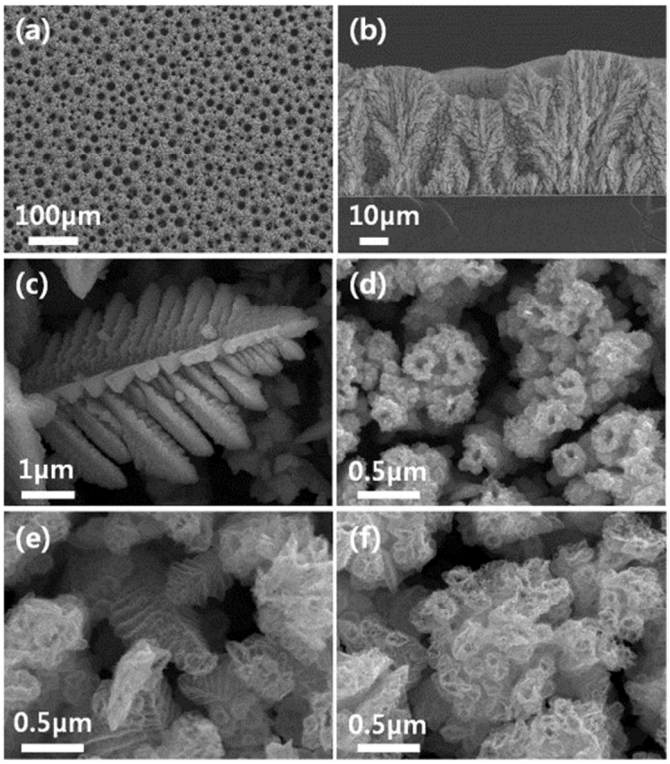

Fig. 8 SEM images of a honeycomb-like RuCu surface showing the overall morphology (a), a cross-sectional view (b) and higher magnification images of the nanostructures before (c-d) and after electrochemical dealloying of the copper (e-f) (Reprinted with permission[66]. Copyright 2012, Elsevier B.V.).

To date the galvanic replacement of copper has centred on the reduction of platinum,[78] palladium,[79] silver[79] and gold.[46] This reflects their activity, as it is known that these can be effective materials for applications such as catalysis, sensing and biological applications, as well the desire to minimise the use of these precious metals due to their cost.

2.3.4 Spontaneous Decoration

Another method of forming bi-metallics on the honeycomb-like structures is through the use of spontaneous decoration procedures. These involve similar procedures to galvanic replacement, with the decoration performed by immersion of the honeycomb-like surface in an appropriate solution under open circuit potential conditions. This was first reported by O'Mullane and Bhargava for the decoration of honeycomb-like gold with Ag, Pd and Pt.[47b] As can be seen from the SEM images in Fig. 9, nanoparticles of Ag (Fig. 9a-b) or Pd (Fig. 9c-d) are visible on the dendritic honeycomb-like gold supports. Such decoration was performed without the aid of commonly employed sources of metal reduction such as the addition of a reductant, the application of an applied potential or through the photoreduction of the metal salts. Instead it was found that the facile oxidation of gold at defect sites (occurring at potentials less positive than the oxidation of bulk gold atoms) provided

sufficient driving force to reduce the metal salts, which is similar to galvanic replacement but results in the growth of nanoparticles or submonolayers on the surface rather than the replacement of the sacrificial metal template. Evidence for the Au oxidation being responsible for the decoration was seen in a range of electrochemical investigations using FT voltammetry, confirming that faradaic processes leading to oxide formation are responsible for the surface active sites. These oxidation responses occur at potential values lower than[80] that for the formation of the compact monolayer oxide of bulk gold, and are assigned to the oxidation of surface active sites. Several electrocatalytic reactions were explored in which the onset potential is aligned with these surface active sites. The facile oxidation of active sites is used to drive the electroless deposition of metals such as palladium and silver from their aqueous salts on the surface of honeycomb Au. These active sites corresponded to surface oxidation species at potentials of ca. 0.29, 0.55 and 1.08 V vs Ag/AgCl, which are considerably more cathodic than the main monolayer oxidation of Au with an onset potential of 1.20 V.

Similar work was also presented by Cherevko and co-workers, who investigated the spontaneous decoration of Pt and Pd on honeycomb-like gold formed through the DHBT method, or on gold electrodes electrochemically activated by vigorous hydrogen evolution.[49b]

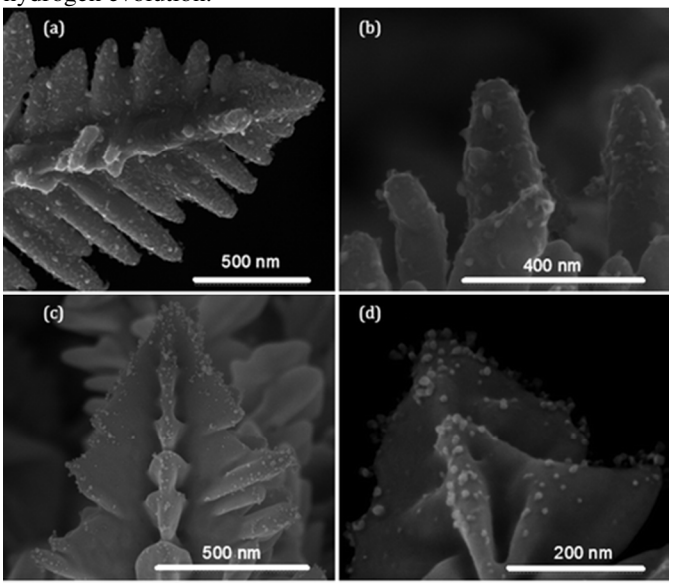

Fig. 9 Honeycomb-like gold surfaces after spontaneous decoration with Ag (a-b) or Pd (c-d) (Reprinted with permission[47b]. Copyright 2011, The Royal Society of Chemistry).

Apart from the decoration of porous structures with noble metals, work has also been performed on their decoration with organic charge transfer molecules. This is illustrated through the decoration of honeycomb-like copper surfaces with 7,7,8,8-tetracyanoquinodimethane (TCNQ) or its fluorinated version ($TCNQF_4$).[35f] The decoration of the latter species is shown in Fig. 10, where the overall porous nature of the honeycomb-like copper electrodeposited for 5 s (Fig. 10 b1) or 10 s (Fig. 10 c1) is still maintained throughout the reaction. Upon closer inspection (Fig. 10 b2 and c2) the pore walls are thicker after the decoration, and a large number of flake-like structures can be seen protruding from the surface (Fig. 10 b3 and c3). Such structures are the result of the formation of $CuTCNQF_4$, where the oxidation of copper is linked to the reduction of $TCNQF_4$ to $TCNQF_4^-$.

3. Emerging Applications of Honeycomb-like Films

There is now an increasing appreciation in the literature that the morphology of surfaces on the nanoscale can significantly affect behaviour in applications, through control of optical, catalytic, electrocatalytic, electronic and mechanical properties. The following sections presents selected examples where the DHBT method is being used to create films for specific applications. The ability to create macroporous surfaces of high specific area due to H_2 templating, coupled with a diverse nanostructures, is an ideal recipe for tailored surfaces for specific applications.

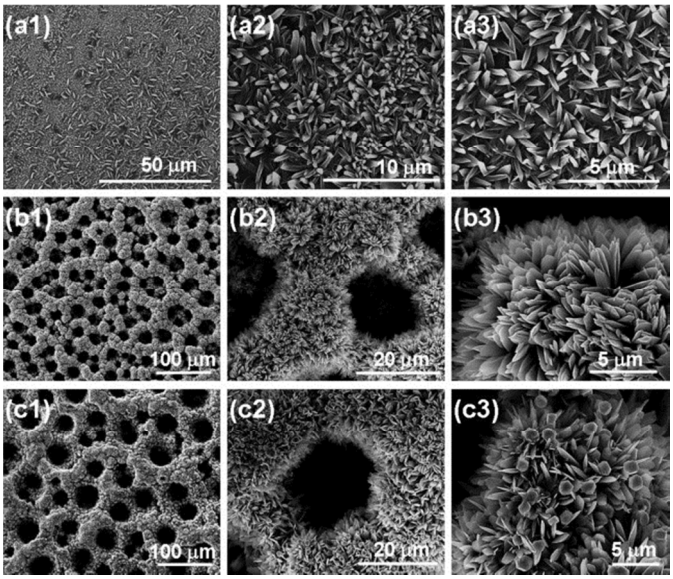

Fig. 10 SEM images of $CuTCNQF_4$ modified surfaces formed by the spontaneous reaction of $TCNQF_4$ with planar copper (a1-3) or honeycomb-like copper electrodeposited for 5 s (b1-3) or 10 s (c1-3) (Reprinted with permission[35f]. Copyright 2012, Elsevier Ltd.).

3.1 Li Batteries

Honeycomb-like Cu structures have been evaluated as current collectors in the anode of lithium batteries as an alternative to graphite anodes. Porous copper deposited by DHBT has been used as the substrate with Sn and Sn based intermetallics deposited on top, and compared to copper foil. Pores increase the surface area and allow for expansion of the anode during cycling. The groups of Kwon and Huang/Sun and co-workers[81] showed, through using this strategy, that Li capacity and cycle performance improved compared to a Cu foil. Control of Cu morphology between grape-like deposits[81b] and dendrites[81c] showed the versatility of morphological control by adjustment of the Cu electrodeposition conditions, with the

grape-like deposits being more structurally sound during cycling. Kang and co-workers[82] deposited Si first onto the porous Cu, for a Si/Cu electrode with a high reversibly capacity and cycling stability. This material was able to be used directly as an anode without other conductive additives or binders.

Sun and co-workers have also expanded the method to Co,[83] depositing an Sn-Co alloy onto porous Cu to obtain a $CoSn_3$ intermetallic that also showed superior cyclability and capacity in comparison to a flat copper foil. Chung and co-workers prepared a Ni-Sn anode for a Li battery, with several compositions of the Ni-Sn alloy being tested[84] with excellent cycle life stability. A nano-Ni/NiO nanoflake composite was reported by Yan and co-workers, with NiO nanoflakes directly anchored onto 3D porous Ni film prepared by DHBT,[85] which showed better performance than a commercial Ni foam, and improved mechanical stability. Improved electrochemical performance was once again confirmed to be due to the highly porous, conducting architecture of the Ni material.

Using honeycomb Cu as the current collector is perhaps the most efficient and easy way to create copper current collectors for lithium batteries with a high surface area. The control of pore size and wall thickness, through our increasing understanding of the parameters that affect films by the DHBT technique has led to retained capacities more than 3 times that of smooth Cu foil.[39]

3.2 Capacitors

High performance capacitors are usually designed with materials of a high specific surface area to ensure maximum contact with the electrolyte. The DHBT method is an alternative to anodic deposition, or solution based synthetic methods such as sol gel. A form of post treatment, such as annealing is usually necessary to convert the metal to an oxide with pseudocapacitive properties. Eugenio and co-workers recently prepared Ni-Cu foams by this method,[86] and Wang and co-workers,[87] generated nano porous Ni which acted as a scaffold, to anchor $Co(OH)_2$ nanoparticles and create a composite electrode. The $Co(OH)_2$ had a high specific capacitance of 1920 F/g, with good cycling stability, with the porous Ni established as a better substrate than commercial Ni foam. Cherevko and co-workers deposited a high surface area Ru-Cu material (Fig. 7),[88] followed by electrochemical de-alloying of the copper and annealing for RuO_x materials with a specific capacitance of 809 F/g, a very competitive value compared to other methods such as sol-gel and hydrothermal processes, and good stability to cycling (~98 % after 300 cycles). In this case high surface area is imparted in two steps – the initial DHBT and then the de-alloying to generate a nanoporous material. A key advantage quoted by the authors is that due to the simplicity of the DHBT technique and the durability of the film, is that it is easily applicable to industrial manufacturing in comparison with the other techniques. These examples demonstrate that capacitors with high performance can be prepared using the DHBT technique to control the initial chemistry and porosity. Due to the relatively few examples so far presented, there is scope to include more chemistries, and the precise control of the nanostructure of thin layers may lead to an improved specific capacitance to those so far observed. There is also scope to apply the technique to improve current collectors for capacitors in a similar way to Li batteries, with appropriate control between the active material and current collector.[89]

3.3 Electrocatalysis: Fuel oxidation

Electrocatalysis for applications in fuel cells has been studied predominately for noble metals such as Pt or noble metal alloys, with morphological control of supported nanoparticles leading to enhanced current densities and stability.[8] Generation of materials by the DHBT method is further improving our understanding of morphological effects on the oxidation of organic alcohols and acids. Bulk materials, if they are of sufficient specific surface area and activity, may show good long-term stability in comparison to supported nanoparticles. Studies on these films invariably correct electrocatalytic current densities for area, and as such, a direct improvement is seen in current density due to the morphology of the film that is formed.

Our group deposited porous Pt directly from a Pt(II) salt[90] which showed higher current density for MeOH oxidation than a flat polycrystalline electrode, and it was proposed that defects and step sites induced during electrodeposition by the DHBT were effective in limiting the surface poisoning by CO. Such surface defects and active sites on the surface may be created as a consequence of the vigorous hydrogen bubbling during deposition.[91] These active sites are prime candidates for further decoration, and can lead to materials with improved catalytic performance. These spontaneous decoration procedures (Fig. 8), have shown that active sites on Au could be decorated with Pt, Pd and Pt.[80, 92] Pt/Au films were shown to be about 25 times more reactive for ethanol oxidation that Pt by this method.

Zelin and co-workers confirmed the synergistic effect of Au and Pt for MeOH oxidation[40] by direct deposition of a bimetallic AuPt honeycomb structure. It was shown how the honeycomb structures could be tuned conveniently in composition to favour either formic acid or methanol oxidation, with a $Au_{100}Pt_1$ surface best for formic acid oxidation (see fig 11), and $Au_{100}Pt_{6\text{-}8}$ films superior for methanol oxidation. Significant improvement are seen over a commercial Etek-Pt/C catalysts (shown in fig. 11 as a dotted line)

Cherevko and co-workers deposited nanoporous Pd[93] which was composed of dendrites with branches of approximately 10 nm in size, having roughness factors of over 1000, and specific surface area of 60 m^2/g. High activity towards C2 alcohols (ethanol and ethylene glycol) was observed, and a key feature is that the relatively inert (slow deposition kinetics) of Pd could be overcome with vigorous H_2 evolution to drive dendritic growth. Chung also prepared porous Pd films,[94] with different pore sizes, that showed different electrocatalytic stability during ethanol oxidation, with current decaying faster on films with small pores in alkaline medium. Incorporation of Ni into Pd by Yu and co-workers[95] was shown to increase the current density for methanol oxidation in basic solution.

Cherevko and co-workers prepared Au_xCu_{100-x} foams, with smaller ligament or particle sizes compared to monometallic foams.[96] Small amounts of Cu greatly improved the stability of the structure in either air or an acidic environment. Displacement of Cu by Pt leads to active catalysts for methanol oxidation in basic solution of the type $Pt@Au_xCu_{100-x}$. It was found that Au enriched surfaces are more active for methanol oxidation, but that Pt enriched surfaces are more stable, and the versatility of the DHBT technique is shown by convenient trade off between the two. Zhu and co-workers also undertook displacement of porous Cu with Pt[97] to create a catalyst for methanol oxidation.

Li and co-workers[98] prepared PtPd alloy foams comprising of nanodendrites for methanol and ethanol oxidation, exploiting the synergistic effect of Pd and Pt to reduce poisoning. Ojani and co-workers systematically[99] varied quantities of Pt and Pd in a porous structure for MeOH and formic acid oxidation. It was found that Pt_3Pd_1 was best for methanol, with a higher activity than pure Pt. This same group[100] showed that a Cu/Pd porous structure showed high current density for formic acid oxidation after galvanic replacement on the porous Cu by Pd. Pd nanostructures[52a] ranging from nano-buds to nanodendrites created by the DHBT method were tested by Huang and co-workers for the oxygen reduction reaction (ORR), with a significant positive shift observed for the new surfaces.

At this stage, making films of precious metals such as Pt and Pd by the DHBT method has not rivalled the best performing shape controlled nanoparticles for specific activity, though highly porous films are candidates for catalysts in fuel cells without a carbon support, and may be a viable alternative to supported nanoparticles in some configurations of fuel cells.

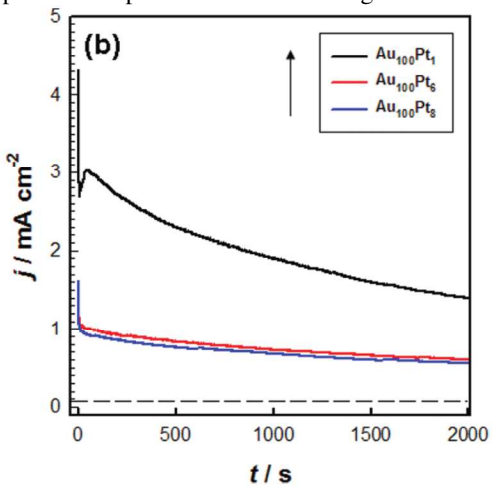

Fig. 11 Chronoamperometric curve of 0.5 M formic acid in 0.5 M H_2SO_4 at -0.315 V for 3D porous films of AuPt. Dotted line is the steady current density of a commercial Pt/C catalyst. Reprinted with permission.[40] Copyright ACS 2011.

3.4 Sensing Applications

Non-enzymatic glucose sensors[101] may show better long term stability than those based on immobilised enzymes, and CuO has been identified as an ideal material. A high surface area of the active material for such sensors would be ideal as it would lead to increased sensitivity.

Cherevko and co-workers prepared a porous CuO electrode[102] by annealing honeycomb Cu deposited by DHBT for non-enzymatic glucose detection. They obtained a sensitivity of 2.9 mA cm^{-2} mM^{-1}, and a detection limit of 0.14 μM. Good selectivity was observed over ascorbic acid and uric acid, with acceptable long-term stability. Bin and co-workers[103] also used annealed honeycomb Cu as a nonenzymatic glucose detector to obtain a material with a 0.8 μM detection limit, and good selectivity against organic acids. Lan and co-workers[104] showed that three-dimensional dendritic structures of high specific surface area (80.8 m^2/g) prepared by DHBT showed significant enhancement of glucose electrooxidation in neutral media, reaching approximately 1.5 times the mass activity of alloys that were obtained by traditional electrochemical techniques. Lorenzo and co-workers[105] prepared porous gold microelectrodes on thin film (100 nm thick) gold substrates, demonstrating possible applicability to microfluidic devices or lab on a chip sensors. A detection limit of 5 μM was observed for glucose, with maltose, lactose and galactose also showing high sensitivity (see figure 12). Films obtained by the DHBT are thus obtaining sensitivity within the limits of glucose in the blood. The primary advantage of these films over nanoparticles or other nanostructures is their mechanical stability.

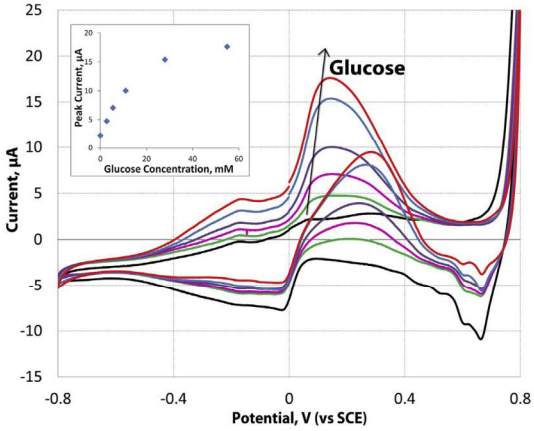

Fig 12 Cyclic voltammetry and calibration curve (inset) of a porous gold electrode at increasing glucose concentrations of 0.0, 2.8, 5.5, 11, 28, 55 mM in PBS. Reproduced with permission[105], copyright Elsevier 2014.

Although glucose sensing has received most attention, some other analytes are emerging as targets. Chung and co-workers[106] used a Au surface, with nanodendrites generated during the DHBT in the presence of iodide, to sense As(III). Peak intensities for the nanodendrite electrode were approximately 40 times higher than for a nanoparticle electrode. Hong and co-workers[107] generated a porous Sn foam structure, and found that after annealing to SnO_2, the pore structure was preserved. The resulting sensor was particularly responsive to ethanol, and also responded to H_2, CO, NH_3 and

NO_x gases. Lee and co-workers[108] functionalised a porous Au electrode with a thin layer of poly (thiophene acetic acid) (PTAA) to immobilise a Pb^{2+} recognising peptide which operated in nM concentration ranges. In an interesting attempt to create a porous matrix for a biosensor, Xia and co-workers[109] created a porous silica matrix formed using electrochemically generated bubbles, incorporating HRP (Horseradish peroxidase) into the matrix which was shown to retain bioactivity. These immobilised HRP molecules were uniformly distributed throughout the matrix. It was suggested that relative simplicity of the process was helpful in preventing denaturation of the enzymes.

Honeycomb Au showed considerable anisotropic growth within its wall structure, which makes it a candidate for Surface Enhanced Raman Spectroscopy (SERS) activity.[47a] Figure 13 shows the signal of Rhodamine B on honeycomb Au, with the SERS signal showing significant enhancement compared to the flat substrate and the powder blank. It was deduced that the sharp tips at the end of dendritic branches were responsible for the significantly enhanced signal.

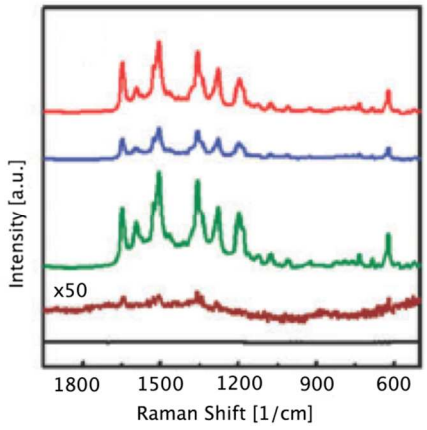

Fig 13. SERS Activity of Rhodamine B on Honeycomb Au deposited for 5 s (green), 10 s (blue) and 30 s (red), unmodified substrate (black) and Rhodamine B powder (brown). Reproduced with permission [47a] copyright RSC.

3.5 Catalytic Applications

In addition to the potential applications in oxidation in fuel cells outlined above, porous films created by DHBT are ideal candidates for further catalytic applications. The hydrogen evolution reaction (HER) is particularly sensitive to surface structure and electronic effects of the metal or alloy.

Chialvo and co-workers[110] found that macroporous nickel did not show large variations where Ni was deposited under a variety of conditions. Perez[111] showed that macroporous Ni, Co and Ni-Co electrodes showed higher catalytic activity for HER in alkaline solution than a smooth commercial Ni electrode. Increasing the Co content resulted in lower roughness but a higher intrinsic HER activity.

O'Mullane and co-workers[112] used a porous Cu/Ag surface for heterogeneous catalysis. HER was found to be sensitive to the nature of the surface, with the HER decreasing with higher Ag loading as expected from the volcano curve. Two catalytic reactions were tested, namely reduction of ferricyanide ions with thiosulphate, and reduction of 4-nitrophenol with $NaBH_4$ in aqueous solution. Ag had a positive effect on both reactions, but was more pronounced in promoting the nitrophenol reduction. The cationic sites on catalysis of Cu-Au surfaces was also studied.[113] It was found that co-electrodeposition resulted in a bimetallic oxide surface, with Au(I) species incorporated into a Cu_2O matrix. The material produced was very efficient for nitrophenol reduction with a low Au loading.

3.6 Superhydrophobicity

Porous films can show superhydrophobic behaviour due to the interaction of the surface morphology with water. A combination of micro and nanostructures is often used to induce superhydrophobicity on a surface, trapping air pockets beneath the water bubble in a lotus leaf effect.[4]

Jiang and co-workers[114] used porous Cu functionalised with thiols to generate surfaces with good dynamic stability, and advancing contact angles above 150°, which was attributed to a combination of dendrites and micron sized pores. Xia and co-workers found, by preparing a range of Cu films,[115] that the hydrophobicity could be tuned by adjusting the wall thickness and pore size, which were dependent upon the electrodeposition conditions. In this case, including a surfactant in the deposition bath had an influence on the bubble behaviour and subsequent morphology, and was able to be used to vary the hydrophobicity (see figure 14). Contact angles up to 160° after surface functionalisation with n-hendecanethiol were observed. O'Mullane/Bhargava and co-workers[116] reacted porous copper with TCNQ and $TCNQF_4$ to form superhydrophobic surfaces with contact angles as large as 177°. CuTCNQ and its derivatives have applications in electronic materials, and making films that are superhydrophobic may be beneficial for moisture resistant devices.

Zelin and co-workers[117] found that porous Sn/SnOx films formed spontaneously by self passivation of porous dendritic Sn while exposed to air, and gave contact angles up to 165° without any organic surface modifications.

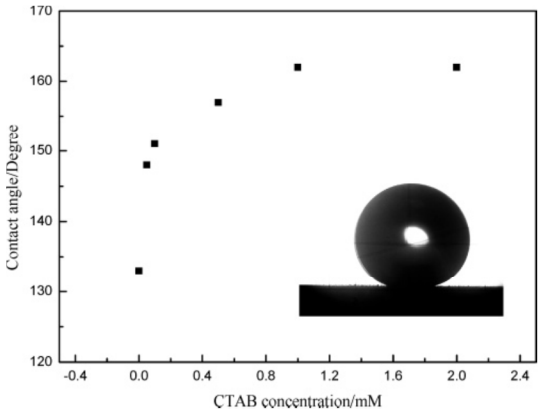

Fig. 14 Water contact angle on the surface or porous copper films electrodeposited with varying CTAB concentrations. Reprinted with permission [115] copyright RSC.

4. Summary and Outlook

What began as a fascinating way to create porous structures of base metals such as Cu and Ni is developing into a versatile technique to construct a range of highly useful materials, with a range of applications that are still growing. One of the key advantages of the DHBT technique is that the most important structural and electronic factors that are considered essential for catalysis, sensing, energy and surface hydrophobicity are simultaneously met, all in a convenient and rapid technique. In the same way that supported nanoparticle work[118] has progressed to allow control of morphology and composition of metal based materials, we hope that the DHBT method may proceed in a similar way, leading to controlled preparation of a broader range of high surface area films. The fundamentals of bubble behaviour and growth of metallic films are now understood to a level that allows films to be prepared with reasonable control of morphology, by adjustment of key parameters for most metals of interest with significant scope for extension to further multi-metallic films.

At this point, genuinely new applications that have been carefully studied are still in their infancy. Recent papers outlined in this feature article have shown that surface confined processes, controlled by a combination of the surface morphology and electronic properties of the film, will hopefully progress beyond the use of model reactions such as HER and fuel oxidation, or processes such as oxygen, ferricyanide or nitrophenol reduction. Important though these processes are, we see potential of the DHBT method to generate surfaces with new and interesting modes of activity. It has already been shown that key metals such as Ru and Pd can be forced into growth structures that are not easily achieved by conventional electrodeposition, and that fascinating structures and chemistries of bimetallic films are accessible through the extreme conditions present during concomitant electrodeposition and H_2 evolution. Dendritic growth, active sites, and surfaces with defects, are all able to be generated readily, giving access to wide ranging surface morphologies with potential for post-deposition treatments. The creation of new materials, such as, for example, cationic Au(I) species incorporated into a Cu_2O matrix, suggests that novel and unusual materials are accessible.

The open porosity of the surfaces, combined with controlled nano-morphology makes these films ideal for catalysis in a range of phases (gas, liquid, electrode/solution interface), or further applications where a porous inorganic material is advantageous. The "Stack up Model" predicts larger surface pores, leading to smaller internal pores in the honeycomb-like structure, allowing improved mass transport of reactants and products to and from the surface, which is desirable in catalysis, electrocatalysis or photocatalysis.

The simplicity and elegance of a one step procedure that directly generates active morphologies is thus a major advantage over methods that require a template or involve de-alloying, and an advantage of the DHBT technique over sol gel or hydrothermal methods is that the pore size and morphology can be reasonably easily controlled by adjustments of the solution chemistry and electrochemical parameters.

An increasing understanding of the overall technique, where H_2 evolution and nucleation and growth of the film are in delicate balance, is leading to a broad range of systematic studies on material development. We can see that improved performance is possible in all of the emerging applications that we have identified – with new applications to follow. These films may be an alternative to supported nanoparticles in key applications, with high active surface area and long term stability provided by the honeycomb-like structure, and fascinating surface chemistry and nano-morphology leading to new or improved activity.

Acknowledgements

LAJ thanks RMIT University for receipt of a Vice Chancellors (Industry) Fellowship. We thank Ahmad Esmaielzadeh Kandjani (RMIT) for generating the images used in the graphical abstract.

References

1 C. M. A. Parlett, K. Wilson and A. F. Lee, *Chem. Soc. Rev.*, 2013, **42**, 3876.
2 A. Walcarius, *Ana.l Bioanal. Chem.*, 2010, **396**, 261.
3 Y. Li, Z.-Y. Fu and B.-L. Su, *Adv. Funct. Mat.*, 2012, **22**, 4634.
4 X.-M. Li, D. Reinhoudt and M. Crego-Calama, *Chem. Soc. Rev.*, 2007, **36**, 1350.
5(a) A. D. Carbó, *Electrochemistry of porous materials*, CRC press, 2010; (b) Y. Wang, X. Wang, M. Antonietti and Y. Zhang, *ChemSusChem*, 2010, **3**, 435; (c) Y. Zhang, Z. Schnepp, J. Cao, S. Ouyang, Y. Li, J. Ye and S. Liu, *Sci. Rep.*, 2013, **3**.
6 K.-S. Choi, *Dalton Trans.*, 2008, 5432.
7 L. P. Bicelli, B. Bozzini, C. Mele and L. D'Urzo, *Int. J. Electrochem. Sci*, 2008, **3**, 356.
8 N. Tian, Z.-Y. Zhou, S.-G. Sun, Y. Ding and Z. L. Wang, *Science*, 2007, **316**, 732.
9 I. Gurrappa and L. Binder, *Science and Technology of Advanced Materials*, 2008, **9**, 043001.
10(a) J. K. Nørskov, T. Bligaard, A. Logadottir, J. R. Kitchin, J. G. Chen, S. Pandelov and U. Stimming, *J. Electrochem. Soc.*, 2005, **152**, J23; (b) S. Trasatti, *J. Electroanal. Chem. and Interfac. Electrochem.*, 1972, **39**, 163.
11 H. Vogt, Ö. Aras and R. J. Balzer, *Int. J. of Heat and Mass Trans.*, 2004, **47**, 787.
12 N. D. Nikolic, K. I. Popov, L. J. Pavlovic and M. G. Pavlovic, *J. Solid State Electrochem.*, 2007, **11**, 667.
13 J. Durst, A. Siebel, C. Simon, F. Hasche, J. Herranz and H. A. Gasteiger, *Energy & Environ. Science*, 2014, **7**, 2255.
14 Y. Ito, T. Ohmori, S. Nakamatsu and S. Yoshizawa, *J. Applied Electrochem.*, 1980, **10**, 419.
15(a) H. Vogt, *J. Applied Electrochem.y*, 1989, **19**, 713; (b) H. Vogt and R. J. Balzer, *Electrochim. Acta*, 2005, **50**, 2073; (c) H. Vogt, *Electrochim. Acta*, 2011, **56**, 1409; (d) *Electrochim.a. Acta*, 2011, **56**, 2404; (e) *Electrochim. Acta*, 2012, **78**, 183.
16 M. Tawfik and F. Diez, *Electrochim. Acta*, 2014, **146**, 792.
17 P. Maciel, T. Nierhaus, S. V. Damme, H. V. Parys, J. Deconinck and A. Hubin, *Electrochem. Commun.*, 2009, **11**, 875.
18 Y. Liu and S. Dillon, *Chem. Commun.*, 2014, **50**, 1761.

19 D. Fernández, P. Maurer, M. Martine, J. M. D. Coey and M. E. Möbius, *Langmuir*, 2014, **30**, 13065.
20 S. Van Damme, P. Maciel, H. Van Parys, J. Deconinck, A. Hubin and H. Deconinck, *Electrochem.y Commun.*, 2010, **12**, 664.
21 L. J. Janssen and J. Hoogland, *Electrochim. Acta*, 1970, **15**, 1013.
22 P. Kristof and M. Pritzker, *J.Applied Electrochem.*, 1997, **27**, 255.
23 W. L. Tsai, P. C. Hsu, Y. Hwu, C. H. Chen, L. W. Chang, J. H. Je, H. M. Lin, A. Groso and G. Margaritondo, *Nature*, 2002, **417**, 139.
24 H. Zhang, Y. Ye, R. Shen, C. Ru and Y. Hu, *J. Electrochem. Soc.*, 2013, **160**, D441.
25 N. D. Nikolić, K. I. Popov, L. J. Pavlović and M. G. Pavlović, *Surf. Coat. Tech.*, 2006, **201**, 560.
26 *J. Electroanal. Chem.*, 2006, **588**, 88.
27 S. Cherevko, N. Kulyk and C. H. Chung, *Nanoscale*, 2012, **4**, 103.
28(a) C. T. J. Low and F. C. Walsh, *Surf. Coat. Tech.*, 2008, **202**, 3050; (b) M. Yang, *J. Mater. Chem.*, 2011, **21**, 3119.
29(a) K. I. Popov, M. G. Pavlović, M. D. Maksimović and S. S. Krstajić, *J. Appl. Electrochem.*, 1978, **8**, 503; (b) K. I. Popov, M. D. Maksimović, D. T. Lukić and M. G. Pavlović, *J. Appl. Electrochem.*, 1980, **10**, 299.
30(a) C. A. Marozzi and A. C. Chialvo, *Electrochim. Acta*, 2001, **46**, 861; (b) *Electrochim. Acta*, 2000, **45**, 2111.
31 D. Grujicic and B. Pesic, *Electrochim. Acta*, 2002, **47**, 2901.
32 H.-C. Shin and M. Liu, *Chem. Mater.*, 2004, **16**, 5460.
33(a) N. D. Nikolić, ed. S. S. Djokić, Springer US, 2012, pp. 187-249; (b) N. D. Nikolić and K. I. Popov, ed. S. S. Djokic, Springer New York, 2010, pp. 1-70.
34(a) N. Nikolić, G. Branković, V. Maksimović, M. Pavlović and K. Popov, *J. Solid State Electrochem.*, 2010, **14**, 331; (b) N. Nikolic, V. Maksimovic, M. Pavlovic and K. Popov, *J. Serb. Chem. Soc.*, 2009, **74**, 689; (c) N. D. Nikolic, G. Brankovic, M. G. Pavlovic and K. I. Popov, *J. Electroanal. Chem.*, 2008, **621**, 13; (d) N. Nikolić, L. J. Pavlovic, M. G. Pavlovic and K. Popov, *J. Serb. Chem. Soc.*, 2007, **72**, 1369; (e) X. Yao, L. Xu and L. Jiang, *Adv. Funct. Mater.*, 2010, **20**, 3343; (f) N. D. Nikolić, L. J. Pavlović, M. G. Pavlović and K. I. Popov, *Electrochim. Acta*, 2007, **52**, 8096; (g) N. D. Nikolic, L. J. Pavlovic, S. B. Krstic, M. G. Pavlovic and K. I. Popov, *Chem. Eng. Sci.*, 2008, **63**, 2824; (h) D. Fernández, Z. Diao, P. Dunne and J. M. D. Coey, *Electrochim. Acta*, 2010, **55**, 8664; (i) N. Nikolic, L. Pavlovic, G. Brankovic, M. Pavlovic and K. Popov, *J. Serb. Chem. Soc.*, 2008, **73**, 753; (j) N. D. Nikolić, L. J. Pavlović, M. G. Pavlović and K. I. Popov, *Powder Technol.*, 2008, **185**, 195; (k) B. Qi, H. Yang, K. Zhao, M. M. Bah, X. Bo and L. Guo, *J. Electroanal. Chem.*, 2013, **700**, 24.
35(a) N. D. Nikolić and G. Branković, *Mater. Lett.*, 2012, **70**, 11; (b) K. Pang, Y. Hou, W. Wu, S. Tian and N. Sun, *Sci. China Chem.*, 2012, **55**, 1325; (c) K. Tan, M.-B. Tian and Q. Cai, *Thin Solid Films*, 2010, **518**, 5159; (d) D. Nam, R. Kim, D. Han, J. Kim and H. Kwon, *Electrochim. Acta*, 2011, **56**, 9397; (e) R. Kim, D. Han, D. Nam, J. Kim and H. Kwon, *J. Electrochem. Soc.*, 2010, **157**, D269; (f) M. Mahajan, S. K. Bhargava and A. P. O'Mullane, *Electrochim. Acta*, 2013, **101**, 186; (g) J. Suk, D. Y. Kim, D. W. Kim and Y. Kang, *J. Mater. Chem. A*, 2014, **2**, 2478; (h) F. Zhang, Y.-L. Wang, D.-X. Fu, L.-M. Li and G.-F. Yin, *Propell. Explos. Pyrot.*, 2013, **38**, 41; (i) S. Li, R. Furberg, M. S. Toprak, B. Palm and M. Muhammed, *Adv. Funct. Mater.*, 2008, **18**, 2215; (j) S. Cherevko and C. H. Chung, *Talanta*, 2010, **80**, 1371; (k) J.-H. Kim, R.-H. Kim and H.-S. Kwon, *Electrochem. Commun.*, 2008, **10**, 1148; (l) Y. Li, W.-Z. Jia, Y.-Y. Song and X.-H. Xia, *Chem. Mater.*, 2007, **19**, 5758; (m) K. Zhang, L. Wang, C. Luo and G. Liu, *ECS Electrochem. Lett.*, 2013, **2**, C23.
36(a) N. D. Nikolić and G. Branković, *Electrochem. Commun.*, 2010, **12**, 740; (b) N. D. Nikolić, G. Branković and V. M. Maksimović, *J. Electroanal. Chem.*, 2011, **661**, 309; (c) N. D. Nikolić, G. Branković, V. M. Maksimović, M. G. Pavlović and K. I. Popov, *J. Electroanal. Chem.*, 2009, **635**, 111; (d) N. D. Nikolić, G. Branković and K. I. Popov, *Mater. Chem. Phys.*, 2011, **125**, 587.
37 I. Najdovski and A. P. O'Mullane, *Journal of Electroanalytical Chemistry*, 2014, **722–723**, 95.
38 A. Ott, L. A. Jones and S. K. Bhargava, *Electrochem. Commun.*, 2011, **13**, 1248.
39 X.-Y. Fan, F.-S. Ke, G.-Z. Wei, L. Huang and S.-G. Sun, *J. Alloy. Compd.*, 2009, **476**, 70.
40 J. Liu, L. Cao, W. Huang and Z. Li, *ACS Applied Mat. Int.*, 2011, **3**, 3552.
41 X. Niu, H. Zhao, C. Chen and M. Lan, *ChemCatChem*, 2013, **5**, 1416.
42 T. N. Huan, T. Ganesh, K. S. Kim, S. Kim, S. H. Han and H. Chung, *Biosens. Bioelectron.*, 2011, **27**, 183.
43 S. Yang, W.-Z. Jia, Q.-Y. Qian, Y.-G. Zhou and X.-H. Xia, *Anal. Chem.*, 2009, **81**, 3478.
44 S. Cherevko and C.-H. Chung, *Electrochim. Acta*, 2010, **55**, 6383.
45 S. Cherevko, X. Xing and C.-H. Chung, *Electrochem. Commun.*, 2010, **12**, 467.
46 Y. Li, Y.-Y. Song, C. Yang and X.-H. Xia, *Electrochem. Commun.*, 2007, **9**, 981.
47(a) B. J. Plowman, A. P. O'Mullane, P. R. Selvakannan and S. K. Bhargava, *Chem. Commun.*, 2010, **46**, 9182; (b) B. J. Plowman, A. P. O'Mullane and S. K. Bhargava, *Faraday Discuss.*, 2011, **152**, 43.
48 I. Najdovski and A. P. O'Mullane, *J.Electroanalytical Chemistry*, 2014, **722-723**, 95.
49(a) S. Cherevko and C.-H. Chung, *Electrochem. Commun.*, 2011, **13**, 16; (b) S. Cherevko, N. Kulyk and C.-H. Chung, *Electrochim. Acta*, 2012, **69**, 190.
50(a) H. du Toit and M. Di Lorenzo, *Sensor. Actuat. B-Chem.*, 2014, **192**, 725; (b) W. Su, M. Cho, J. D. Nam, W. S. Choe and Y. Lee, *Biosens. Bioelectron.*, 2013, **48**, 263.
51 X. Xing, S. Cherevko and C.-H. Chung, *Mater. Chem. Phys.*, 2011, **126**, 36.
52(a) G.-M. Yang, X. Chen, J. Li, Z. Guo, J.-H. Liu and X.-J. Huang, *Electrochim. Acta*, 2011, **56**, 6771; (b) R. Li, H. Mao, J. Zhang, T. Huang and A. Yu, *J. Power Sources*, 2013, **241**, 660.
53 S. Cherevko, X. Xing and C.-H. Chung, *Appl. Surf. Sci.*, 2011, **257**, 8054.
54 W. Huang, L. Fu, Y. Yang, S. Hu, C. Li and Z. Li, *Electrochem. Solid-State Lett.*, 2010, **13**, K46.
55 J. Liu, L. Cao, W. Huang and Z. Li, *J. Electroanal. Chem.*, 2012, **686**, 38.
56 J.-H. Jeun, D.-H. Kim and S.-H. Hong, *Sensor. Actuat. B-Chem.*, 2012, **161**, 784.
57 L. Cao, J. Liu, S. Xu, Y. Xia, W. Huang and Z. Li, *Mater. Res. Bull.*, 2013, **48**, 4804.
58 D. K. Oppedisano, L. A. Jones, T. Junk and S. K. Bhargava, *J. Electrochem. Soc.*, 2014, **161**, D489.
59 V. D. Jović, V. Maksimović, M. G. Pavlović and K. I. Popov, *J. Solid State Electrochem.*, 2005, **10**, 373.
60 C. González-Buch, I. Herraiz-Cardona, E. Ortega, J. García-Antón and V. Pérez-Herranz, *Int. J. Hydrogen Energy*, 2013, **38**, 10157.
61(a) I. Herraiz-Cardona, E. Ortega, L. Vázquez-Gómez and V. Pérez-Herranz, *Int. J. Hydrogen Energy*, 2012, **37**, 2147; (b) I. Herraiz-Cardona, C. González-Buch, E. Ortega, J. García-Antón and V. Pérez-Herranz, *Chem. Eng. Trans.*, 2013, **32**, 451.
62 D. H. Nam, R. H. Kim, D. W. Han and H. S. Kwon, *Electrochim. Acta*, 2012, **66**, 126.
63 I. Najdovski, P. R. Selvakannan, S. K. Bhargava and A. P. O'Mullane, *Nanoscale*, 2012, **4**, 6298.
64 I. Najdovski, P. R. Selvakannan, A. P. O'Mullane and S. K. Bhargava, *Chem. Eur. J.*, 2011, **17**, 10058.
65 I. Najdovski, P. R. Selvakannan and A. P. O'Mullane, *RSC Adv.*, 2014, **4**, 7207.
66 M.-G. Jeong, K. Zhuo, S. Cherevko, W.-J. Kim and C.-H. Chung, *J. Power Sources*, 2013, **244**, 806.
67 H. C. Shin and M. Liu, *Adv. Funct. Mater.*, 2005, **15**, 582.
68 K. Zhuo, M.-G. Jeong and C.-H. Chung, *J. Power Sources*, 2013, **244**, 601.
69 L. D. Rafailovic, D. M. Minic, H. P. Karnthaler, J. Wosik, T. Trisovic and G. E. Nauer, *J. Electrochem. Soc.*, 2010, **157**, D295.
70 L. Mattarozzi, S. Cattarin, N. Comisso, A. Gambirasi, P. Guerriero, M. Musiani, L. Vázquez-Gómez and E. Verlato, *Electrochimica Acta*, 2014.
71 M. Jin and H. Ma, *Russ. J. Electrochem.*, 2013, **49**, 1081.
72 J. Liu, L. Cao, W. Huang and Z. Li, *ACS Appl. Mater. Interfaces*, 2011, **3**, 3552.
73 S. Cherevko, N. Kulyk and C. H. Chung, *Nanoscale*, 2012, **4**, 568.
74 L. D. Rafailović, C. Gammer, C. Kleber, C. Rentenberger, P. Angerer and H. P. Karnthaler, *J. Alloy. Compd.*, 2012, **543**, 167.
75 X. M. Zheng, L. Huang, Y. Xiao, H. Su, G. L. Xu, F. Fu, J. T. Li and S. G. Sun, *Chem. Commun.*, 2012, **48**, 6854.

76 C. M. Cobley and Y. Xia, *Mat. Sci. and Engineering: R: Reports*, 2010, **70**, 44.
77 X. Xia, Y. Wang, A. Ruditskiy and Y. Xia, *Adv. Mat.*, 2013, **25**, 6313.
78(a) J. Yin, J. Jia and L. Zhu, *Microchim. Acta*, 2009, **166**, 151; (b) J.-B. Raoof, R. Ojani, A. Kiani and S. Rashid-Nadimi, *Int. J. Hydrogen Energy*, 2010, **35**, 452; (c) J. Yin, J. Jia and L. Zhu, *Int. J. Hydrogen Energy*, 2008, **33**, 7444; (d) S. Cherevko, N. Kulyk and C. H. Chung, *Langmuir*, 2012, **28**, 3306.
79 P. Shahbazi and A. Kiani, *Electrochim. Acta*, 2011, **56**, 9520.
80 B. J. Plowman, A. P. O'Mullane and S. K. Bhargava, *Faraday Discuss.*, 2011, **152**, 43.
81(a) L. Huang, H.-B. Wei, F.-S. Ke, X.-Y. Fan, J.-T. Li and S.-G. Sun, *Electrochim. Acta*, 2009, **54**, 2693; (b) D. H. Nam, R. H. Kim, D. W. Han and H. S. Kwon, *Electrochim. Acta*, 2012, **66**, 126; (c) R. Kim, D. Han, D. Nam, J. Kim and H. Kwon, *J. Electrochem. Soc.*, 2010, **157**, D269.
82 J. Suk, D. Y. Kim, D. W. Kim and Y. Kang, *J. Mat. Chem.y A*, 2014, **2**, 2478.
83 X.-Y. Fan, F.-S. Ke, G.-Z. Wei, L. Huang and S.-G. Sun, *J.f Alloys and Compounds*, 2009, **476**, 70.
84 K. Zhuo, M.-G. Jeong and C.-H. Chung, *J. Power Sources*, 2013, **244**, 601.
85 X. Yan, X. Tong, J. Wang, C. Gong, M. Zhang and L. Liang, *Mat. Lett.*, 2013, **106**, 250.
86 S. Eugénio, T. Silva, M. Carmezim, R. Duarte and M. Montemor, *J. Applied Electrochem.*, 2014, **44**, 455.
87 X. H. Xia, J. P. Tu, Y. Q. Zhang, Y. J. Mai, X. L. Wang, C. D. Gu and X. B. Zhao, *J. Phys. Chem. C*, 2011, **115**, 22662.
88 M.-G. Jeong, K. Zhuo, S. Cherevko, W.-J. Kim and C.-H. Chung, *J. Power Sources*, 2013, **244**, 806.
89 P. Simon and Y. Gogotsi, *Nature Mat.*, 2008, **7**, 845.
90 A. Ott, L. A. Jones and S. K. Bhargava, *Electrochem. Commun.*, 2011, **13**, 1248.
91 A. P. O'Mullane and S. K. Bhargava, *Electrochem Commun.*, 2011, **13**, 852.
92 S. Cherevko, N. Kulyk and C.-H. Chung, *Electrochim Acta*, 2012, **69**, 190.
93 I. Najdovski, P. R.Selvakannan, S. K.Bhargava, A.O'Mullane, *Nanoscale*, 2012, 4, 103.
94 X. Xing, S. Cherevko and C.-H. Chung, *Materials Chemistry and Physics*, 2011, **126**, 36.
95 R. Li, H. Mao, J. Zhang, T. Huang and A. Yu, *Journal of Power Sources*, 2013, **241**, 660.
96 S. Cherevko, N. Kulyk and C.-H. Chung, *Langmuir*, 2012, **28**, 3306.
97 J. Yin, J. Jia and L. Zhu, *Int. J. of Hydrogen Energy*, 2008, **33**, 7444.
98 J. Liu, L. Cao, W. Huang and Z. Li, *J. Electroanal. Chem.*, 2012, **686**, 38.
99 R. Ojani, E. Hasheminejad and J. B. Raoof, *Int. J. Hydrogen Energy*, 2014, **39**, 8194.
100 R. Ojani, Z. Abkar, E. Hasheminejad and J.-B. Raoof, *Int. J. of Hydrogen Energy*, 2014, **39**, 7788.
101 J. Wang, *Chem. Rev.*, 2007, **108**, 814.
102 S. Cherevko and C.-H. Chung, *Talanta*, 2010, **80**, 1371.
103 B. Qi, H. Yang, K. Zhao, M. M. Bah, X. Bo and L. Guo, *J. Electroanal.l Chem.y*, 2013, **700**, 24.
104 X. Niu, H. Zhao, C. Chen and M. Lan, *ChemCatChem*, 2013, **5**, 1416.
105 H. du Toit and M. Di Lorenzo, *Sensors and Actuators B: Chemical*, 2014, **192**, 725.
106 T. N. Huan, T. Ganesh, K. S. Kim, S. Kim, S.-H. Han and H. Chung, *Biosensors and Bioelectronics*, 2011, **27**, 183.
107 J.-H. Jeun, D.-H. Kim and S.-H. Hong, *Sens. and Actuators B: Chem.*, 2012, **161**, 784.
108 W. Su, M. Cho, J.-D. Nam, W.-S. Choe and Y. Lee, *Biosens. and Bioelectron.*, 2013, **48**, 263.
109 S. Yang, W.-Z. Jia, Q.-Y. Qian, Y.-G. Zhou and X.-H. Xia, *Anal. Chem.*, 2009, **81**, 3478.
110 C. A. Marozzi and A. C. Chialvo, *Electrochim. Acta*, 2001, **46**, 861.
111 C. González-Buch, I. Herraiz-Cardona, E. Ortega, J. García-Antón and V. Pérez-Herranz, *Int. J. of Hydrogen Energy*, 2013, **38**, 10157.
112 I. Najdovski, P. R. Selvakannan and A. P. O'Mullane, *RSC Advances*, 2014, **4**, 7207.
113 I. Najdovski, P. R. Selvakannan, S. K. Bhargava and A. P. O'Mullane, *Nanoscale*, 2012, **4**, 6298.
114 X. Yao, L. Xu and L. Jiang, *Adv. Funct. Mat.*, 2010, **20**, 3343.
115 Y. Li, W.-Z. Jia, Y.-Y. Song and X.-H. Xia, *Chem. Mat.*, 2007, **19**, 5758.
116 M. Mahajan, S. K. Bhargava and A. P. O'Mullane, *Electrochim. Acta*, 2013, **101**, 186.
117 L. Cao, J. Liu, S. Xu, Y. Xia, W. Huang and Z. Li, *Mat. Res. Bulletin*, 2013, **48**, 4804.
118 R. J. White, R. Luque, V. L. Budarin, J. H. Clark and D. J. Macquarrie, *Chem. Soc. Rev.*, 2009, **38**, 481.

